Nischarin inhibition alters energy metabolism by activating AMP-activated protein kinase

Received for publication, March 2, 2017, and in revised form, August 22, 2017 Published, Papers in Press, August 24, 2017, DOI 10.1074/jbc.M117.784256

Shengli Dong[‡], Somesh Baranwal[‡§], Anapatricia Garcia[¶], Silvia J. Serrano-Gomez[‡‖], Steven Eastlack[‡], Tomoo Iwakuma[**], Donald Mercante[‡‡], Franck Mauvais-Jarvis[§§1], and Suresh K. Alahari[‡2]

From the [‡]Department of Biochemistry and Molecular Biology, School of Medicine, and [‡‡]Department of Biostatistics, School of Public Health, Louisiana State University Health Science Center, New Orleans, Louisiana 70112, the [§]Center for Biochemistry and Microbial Sciences, Central University of Punjab, City Campus Mansa Rd., Bathinda-151001, India, the [¶]Department of Pathology and Laboratory Medicine, Emory University, Atlanta, Georgia 30322, the [‖]Pontificia Universidad Javeriana, 11001000 Bogotá, Colombia, the [**]Department of Cancer Biology, Kansas University Medical Center, Kansas City, Kansas 66160, and the [§§]Division of Endocrinology, Tulane University School of Medicine, New Orleans, Louisiana 70112

Edited by Jeffrey E. Pessin

Nischarin (Nisch) is a key protein functioning as a molecular scaffold and thereby hosting interactions with several protein partners. To explore the physiological importance of Nisch, here we generated Nisch loss-of-function mutant mice and analyzed their metabolic phenotype. Nisch-mutant embryos exhibited delayed development, characterized by small size and attenuated weight gain. We uncovered the reason for this phenotype by showing that Nisch binds to and inhibits the activity of AMP-activated protein kinase (AMPK), which regulates energy homeostasis by suppressing anabolic and activating catabolic processes. The Nisch mutations enhanced AMPK activation and inhibited mechanistic target of rapamycin signaling in mouse embryonic fibroblasts as well as in muscle and liver tissues of mutant mice. Nisch-mutant mice also exhibited increased rates of glucose oxidation with increased energy expenditure, despite reduced overall food intake. Moreover, the Nisch-mutant mice had reduced expression of liver markers of gluconeogenesis associated with increased glucose tolerance. As a result, these mice displayed decreased growth and body weight. Taken together, our results indicate that Nisch is an important AMPK inhibitor and a critical regulator of energy homeostasis, including lipid and glucose metabolism.

Our laboratory previously identified Nischarin, a novel protein that binds preferentially to the cytoplasmic domain of the integrin $\alpha 5$ (1). The Nischarin gene (*nisch*) was subsequently mapped to chromosome 3p21, a metastasis-suppressor locus that is frequently lost in several types of cancer (2). In accordance with this, we have shown that overexpression of Nischarin inhibits breast tumor growth and metastasis (3). Specifically, Nischarin inhibits Rac-induced migration and invasion in breast and colon epithelial cells by inhibiting PAK1 and LIMK1 (4–6). Thus, Nischarin's tumor suppressor activity stems from its ability to regulate cytoskeletal signaling. Furthermore, we found that the LKB1 tumor suppressor interacts with the N terminus of Nischarin and, specifically, that amino acids 416–624 of Nischarin are crucial for this interaction (7). Other known binding partners include Rac1, Rab14, Rab9, and IRS1, -2, -3, and -4 (2). To facilitate the interaction with these numerous binding partners, Nischarin contains multiple domains involved in protein–protein interactions, including a Phox domain, a leucine-rich repeat (LRR) domain, a coiled-coil domain, an integrin-binding domain, a proline-rich domain, and the C-terminal region. Given its association with numerous proteins, we suspect Nischarin functions as a scaffolding protein chiefly involved in mediating extracellular to intracellular signaling.

AMP-activated protein kinase (AMPK)[3] is a heterotrimeric serine/threonine kinase that functions as an intracellular energy sensor and plays a critical role in maintaining energy homeostasis (8). Following a decrease in cell energy substrates, AMPK stimulates ATP-generating catabolic pathways, including glycolysis and uptake of glucose and fatty acids. Furthermore, activated AMPK suppresses ATP-consuming pathways such as lipogenesis and protein synthesis. Under conditions of energy stress, ATP levels fall, leading to rising levels of AMP, which binds to the γ-regulatory subunit AMPK and activates the enzyme allosterically (8). In addition to directly regulating activity of key metabolic enzymes, AMPK also induces gene expression pathways that function to promote catabolic cell

This work was supported in part by the Louisiana State University School of Medicine and the Fred G. Brazda Foundation. The authors declare that they have no conflicts of interest with the contents of this article. The content is solely the responsibility of the authors and does not necessarily represent the official views of the National Institutes of Health.

This article contains supplemental Figs. S1–S11 and Table S1.

[1] Supported by National Institutes of Health Grants R01 DK074970 and DK107444.

[2] To whom correspondence should be addressed: Fred G. Brazda Professor of Biochemistry, Louisiana School of Medicine, CSRB 406, New Orleans, LA 70112. Tel.: 504-568-4734; E-mail: salaha@lsuhsc.edu.

[3] The abbreviations used are: AMPK, AMP-activated protein kinase; mTOR, mechanistic target of rapamycin; MEF, mouse embryonic fibroblast; LRR, leucine-rich repeat; 2-NBDG, 2-[*N*-(7-nitrobenz-2-oxa-1,3-diazol-4-yl) amino]-2-deoxy-D-glucose; AICAR, 5-aminoimidazole-4-carboxamide ribonucleotide; IRAS, imidazoline receptor antiserum-selected; Het, heterozygous; CREB, cAMP-response element-binding protein; PEPCK, phosphoenolpyruvate carboxykinase; Glc-6-P, glucose 6-phosphate; HK, hexokinase; FCCP, carbonyl cyanide 4-(trifluoromethoxy)phenylhydrazone; ECAR, extracellular acidification rate; OCR, oxygen consumption rate; ChREBP, carbohydrate-response element-binding protein; RQ, respiratory quotient; AUC, area under curve; qRT, quantitative RT; FAS, fatty-acid synthase; L-PK, liver pyruvate kinase.

processes while inhibiting anabolic ones (9). Because Nisch interacts with LKB1, we sought to determine to what extent Nisch affects AMPK signaling.

To further understand Nischarin's function and the nature of its protein interactions, we produced Nischarin-mutant mice by deleting the crucial LRR region. The resulting Nischarin mutant animals were characteristically small in size, leading us to hypothesize that Nischarin regulates pathways involved in growth and metabolism. Here, we show that Nischarin interacts with AMPK *in vivo* and thereby regulates its activity. Specifically, our findings revealed that mutating Nischarin resulted in findings indicative of greater overall AMPK activity, including increased glucose tolerance and suppression of lipogenic gene expression.

Results

Mutation of the Nischarin LRR domain in mouse model

More than 60,000 proteins from viruses to eukaryotes contain leucine-rich repeats (LRRs). LRRs have diverse functions; however, chief among them is the facilitation of protein–protein interaction (10–13). The length of LRR motifs is variable, ranging from 20–43 residues. All LRR units contain a highly conserved segment, consisting of L*XX*L*XX*N*X*L or L*XX*L*XX*C*XX*L, in which L represents Leu, Ile, Val, or Phe, N indicates Asn, Thr, Ser, or Cys, and C is usually Cys, Ser, or Asn. According to the length and consensus sequences of six LRRs in Nischarin, the 22-amino acid-long Nischarin LRRs most likely belongs to SDS22-like subfamily.

To investigate the potential role of the Nischarin LRR domain in a physiological context, we generated Nischarin-mutant mice in association with the inGenious Targeting Laboratory (Stony Brook, NY). The targeting vector is designed to delete exons 7–10 (encoding 224–395 amino acids containing five LRRs) with insertion of a neo-cassette floxed by FRT and loxP sequences in intron 6 and another into intron 10 of the endogenous Nischarin locus (supplemental Fig. 1*A*). Appropriate homologous recombination in 129Sv/Ev embryonic stem (ES) cells was confirmed by Southern blotting (supplemental Fig. 1*B*). Successfully targeted ES cells were microinjected into C57BL/6 blastocysts. Resulting chimeras were mated to wild-type C57BL/6 mice to generate F1 heterozygous offspring. Successful germ line transmission of the targeted allele (Tg) was confirmed by PCR using Lox1 and SDL2 (supplemental Fig. 1, *C* and *D*). We crossed these F1 mice (Nc^{Tg}) with C57BL/6 CMV-Flp mice to remove the neo-cassette (Nc^{cond}) (Δneo). We then backcrossed the Nc^{cond} mice to C57BL/6 mice six times to generate F5 Nc^{cond} mice (~97% of *C57BL/6* genetic background). To obtain whole-body Nischarin-mutant mice, we bred these F5 Nc^{cond} mice with C57BL/6 CMV-cre mice to generate Nischarin-mutant ($Nc^{\Delta e7-10}$) allele. The resulting Nischarin-mutant ($Nc^{\Delta e7-10}$) allele produced a truncated Nischarin protein lacking the LRR domain (Fig. 5*A*).

Dramatic growth defect in Nischarin LRR-mutation mice

Nischarin homozygous $Nc^{\Delta e7-10/\Delta e7-10}$ (mutant/mutant) mice were fertile and were born in the expected Mendelian ratio. As described below, mutant mice were reduced in size compared with wild-type animals (Fig. 1*A*). Therefore, we

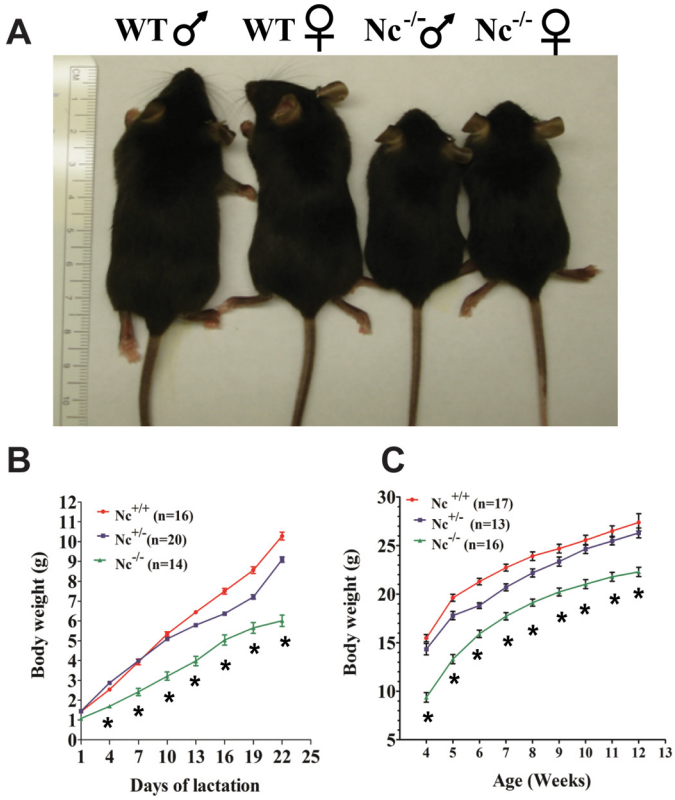

Figure 1. Dramatic growth defect in mice with the LRR mutation of *Nisch* gene. *A*, representative image showing the typical size difference between 4-week-old wild-type (*WT*) $Nc^{+/+}$ and homozygous $Nc^{\Delta e7-10/\Delta e7-10}$ mice. *B*, weight gain curve of WT, heterozygous $Nc^{+/\Delta e7-10}$ (Het), and mutant male mice from birth to 21 days of lactation. *C*, graphical representation of average weight of WT, Het, and mutant male mice from 4 to 12 weeks old. Data represent the mean ± S.E. Student's *t* test was used to analyze the data. WT *versus* Null, *, $p < 0.001$ in *B* and *C*.

decided to examine the size of the embryos. We bred Nischarin heterozygous $Nc^{+/\Delta e7-10}$ (Het) × heterozygous $Nc^{+/\Delta e7-10}$ (Het). The embryos were extracted from gravid females 18.5 days after conception. As shown, the embryos of mutant mice are smaller than their wild-type counterparts (supplemental Fig. 2). Vertical/longitudinal sections were prepared and stained with H&E. Some distinguished differences in the brain, spine, and gut areas among wild-type and homozygous of 18.5-day embryos were noted (supplemental Fig. 3, *A–C*). These differences include reduced brain mass with abnormal organization of both the cerebrum and cerebellum and absence of the oral and nasal cavities (supplemental Fig. 3, *B* and *C*). Also, the gastrointestinal tract failed to completely form in the mutant embryos. Because the size of the animals varied significantly, we measured body weight over a period of 11 weeks (every 3 days during the first 21 days of the lactation period and every week after weaning for an additional 8 weeks). The body weight of male Nischarin Het mice at birth was slightly lower than that of wild-type mice and generally remained low for several weeks before eventually catching up to the wild-type mice at around week 10 (Fig. 1, *A–C*). In the mutant mice, however, the body weight at parturition was lower than that of either the wild-type or the Het mice and remained below normal throughout the entire life span of the animals. Both the male and female Nischarin-mutant mice exhibited dramatic

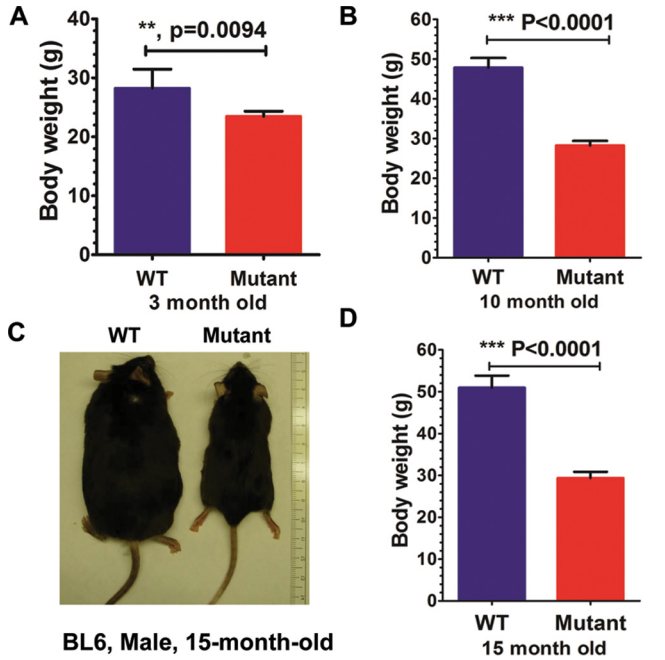

Figure 2. Body weights from 3-month-old (*A*), 10-month-old (*B*), and 15-month-old (*D*) old male mice are shown. *C*, representative image showing the typical size difference between 15-month-old WT and null mice and *D* quantitative data of *C*.

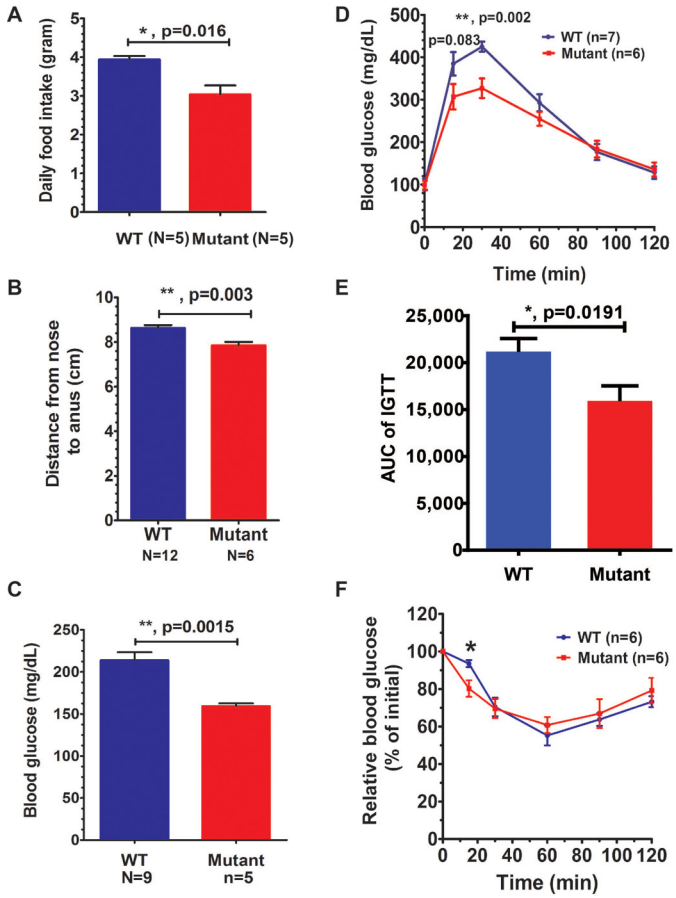

Figure 3. Nischarin LRR mutation alters metabolism in mice. *A*, daily food intake; *B*, distance measurements (from nose to anus); and *C*, blood glucose levels in male 3-month-old Nischarin wild-type and null mice. *D*, glucose tolerance determined using overnight-fasted 3-month-old male mice after an i.p. injection of glucose (1 g/kg body weight). Blood glucose levels were measured at the indicated time points. *E*, area under curve (*AUC*) of IGTT; AUC was calculated above the basal value using the data from *D*. *F*, insulin sensitivity was determined using 5-h-fasted 3-month-old male mice after an i.p. injection of insulin (0.75 IU/kg body weight). Results are indicated as the percentage of initial blood glucose levels.

growth retardation compared with wild-type mice for their entire life. However, the body weight of female Het mice did not show any significant difference from that of the wild-type mice (data not shown). We monitored the wild-type and Nischarin mutant C57BL/6 male mice for over 2 years, during which time the mutant mice remained consistently undersized.

Nischarin LRR-deletion improves energy balance glucose and insulin tolerance

Mutant mice showed a significant decrease in body weight at 3, 10, and 15 months of age compared with WT mice (Fig. 2, *A*–*D*, and supplemental Fig. 4, *A* and *B*). In seeking to account for this, we speculated that a defect in metabolism was a likely source of the growth retardation in the mice. To examine this possibility, we chose to focus on the AMPK-signaling pathway, because it has previously been reported that disruption of LKB1–AMPK–mTOR signaling results in a reduction in mouse body weight, analogous to our observations (14, 15). The decreased body weight in the mutant animals corresponded with a reduction in food intake by the animals (Fig. 3, *A* and *B*). Moreover, blood glucose levels in 3-month-old Nischarin-mutant mice were decreased compared with control (Fig. 3*C*). To test the physiological effects of Nischarin gene deficiency, we examined fasting blood glucose level of wild-type and mutant mice at various time points after i.p. administration of glucose. Mutant animals exhibited improved glucose tolerance (Fig. 3, *D* and *E*). We similarly examined insulin tolerance. Consistent with glucose tolerance data, Nisch-mutant mice were initially insulin-sensitive but gradually became insensitive after 30 min (Fig. 3*F*).

Nischarin interacts with AMPK-α2 in vivo

Given our preliminary findings suggesting that AMPK function is altered in response to the Nischarin mutation status, we hypothesized that AMPK and Nischarin proteins interact. Because the AMPK α subunit is the major catalytic subunit mediating its function, we tested the interaction between AMPK and the LRR domains of Nischarin. Six LRR domains exist in Nischarin, which we deleted to make Nischarin-mutant mice (Fig. 4*A*). FLAG-AMPK and Myc-Nischarin were co-expressed in HEK-293T cells and immunoprecipitated with anti-Myc and blotted with anti-FLAG antibody (Fig. 4*B*). In addition, the lysates were immunoprecipitated with anti-FLAG and immunoblotted with anti-Myc (supplemental Fig. 5*A*). In either fashion, the interaction between Nischarin and AMPK was detected (Fig. 4*B* and supplemental Fig. 5*A*). Also, both proteins co-localized within cells (supplemental Fig. 5*B*). We chose PC12 cells to demonstrate endogenous interaction, as they express a good amount of both AMPK and Nischarin protein. We were able to show the interaction of these endogenous proteins in PC12 cells by Western blotting (Fig. 4, *D* and *E*). To

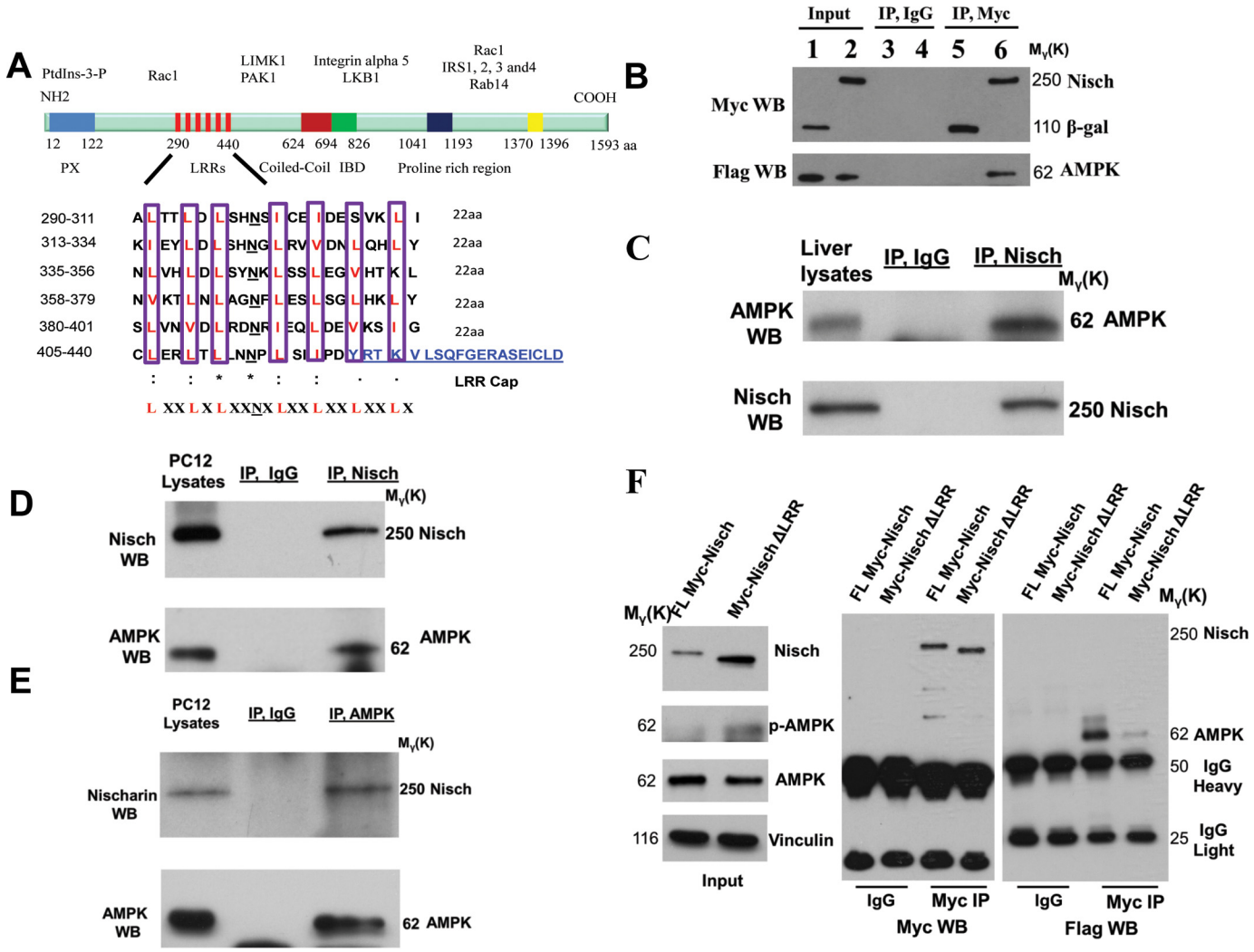

Figure 4. Nischarin interacts with AMPK. *A,* schematic diagram illustrates the molecular organization of Nischarin and its binding partners. The LRRs were deleted in Nisch knock-out mouse. *B,* Myc–Nischarin interacts with FLAG–AMPKα2. 293T cells were co-transfected with Myc–Nischarin and FLAG–AMPKα2 or Myc–β-gal (control vector) and FLAG–AMPKα2. After 48 h, cell lysates were subjected to immunoprecipitation (*IP*) with anti-Myc or control mouse IgG antibodies, followed by Western blot (*WB*) analyses with anti-Myc and anti-FLAG antibodies. *C,* endogenous Nischarin interacts with AMPK in mouse liver. *D* and *E*, endogenous Nischarin interacts with AMPK in PC12 cells. Cell lysates were subjected to immunoprecipitation with anti-Nischarin antibody or control rabbit IgG antibody, followed by Western blot analyses with anti-Nischarin and anti-AMPK antibodies. *F,* overexpression of Myc-NischarinΔLRR in 293T cells increased the level of AMPK Thr-172 phosphorylation. *Left panel*: 293T cells were transiently transfected with Myc-Nischarin (full-length) or Myc-NischarinΔLRR. After 48 h, cell lysates were subjected to immunoblot analysis with anti-Nischarin, anti-pThr-172 AMPK, and anti-AMPK antibodies. Vinculin was used as loading control. *Right panel,* 293 cells were transfected with full-length Myc-Nisch + FLAG AMPK or Myc-Nisch ΔLRR + FLAG-AMPK, and the lysates were immunoprecipitated with anti-Myc and blotted with IgG, anti-Myc, and anti-FLAG. *, $p < 0.05$; **, $p < 0.01$.

further validate this interaction in a physiological setting, we tested the interaction in the mouse liver and adipose tissue, which are key players in body metabolism. Once again, endogenous Nisch and AMPK proteins were found to interact in liver (Fig. 4*C*) and adipose tissue lysates (data not shown). As expected, we did not detect any endogenous Nisch and AMPK protein interaction in Nischarin mutant liver lysates (supplemental Fig. 5*C*). These data suggest that Nischarin interacts with AMPK.

To study this interaction more closely, we prepared a construct that lacks the LRR domain and examined the effect on phosphorylation of AMPK. Deletion of the LRR domain from Nischarin resulted in an increase in AMPK phosphorylation (Fig. 4*F*, *left panel*), suggesting that Nischarin binding to AMPK inhibits its activation. Furthermore, LRR-deleted Nischarin exhibited weak binding to AMPK (Fig. 4*F*, *right panel*) suggesting that LRR domain is essential for Nischarin binding as well as inhibiting AMPK.

Nischarin LRR deletion increases AMPK output in mouse embryonic fibroblasts (MEFs)

To further examine the function of Nischarin, we generated wild-type, heterozygous, and homozygous Nischarin mutant MEFs at the 13.5-embryonic day as described previously (16). Mutant MEFs exhibited the same size as the wild-type MEFs based on our FACS analysis, and no changes in cell proliferation were detected (supplemental Fig. 6, data not shown). Consistent with cell proliferation data, there were no major differences in the cell cycle profiles (supplemental Fig. 7).

As described above, Nischarin-mutant mice are smaller than their wild-type counterparts. One likely source of the growth defect could be the disruption of normal metabolism (17). As

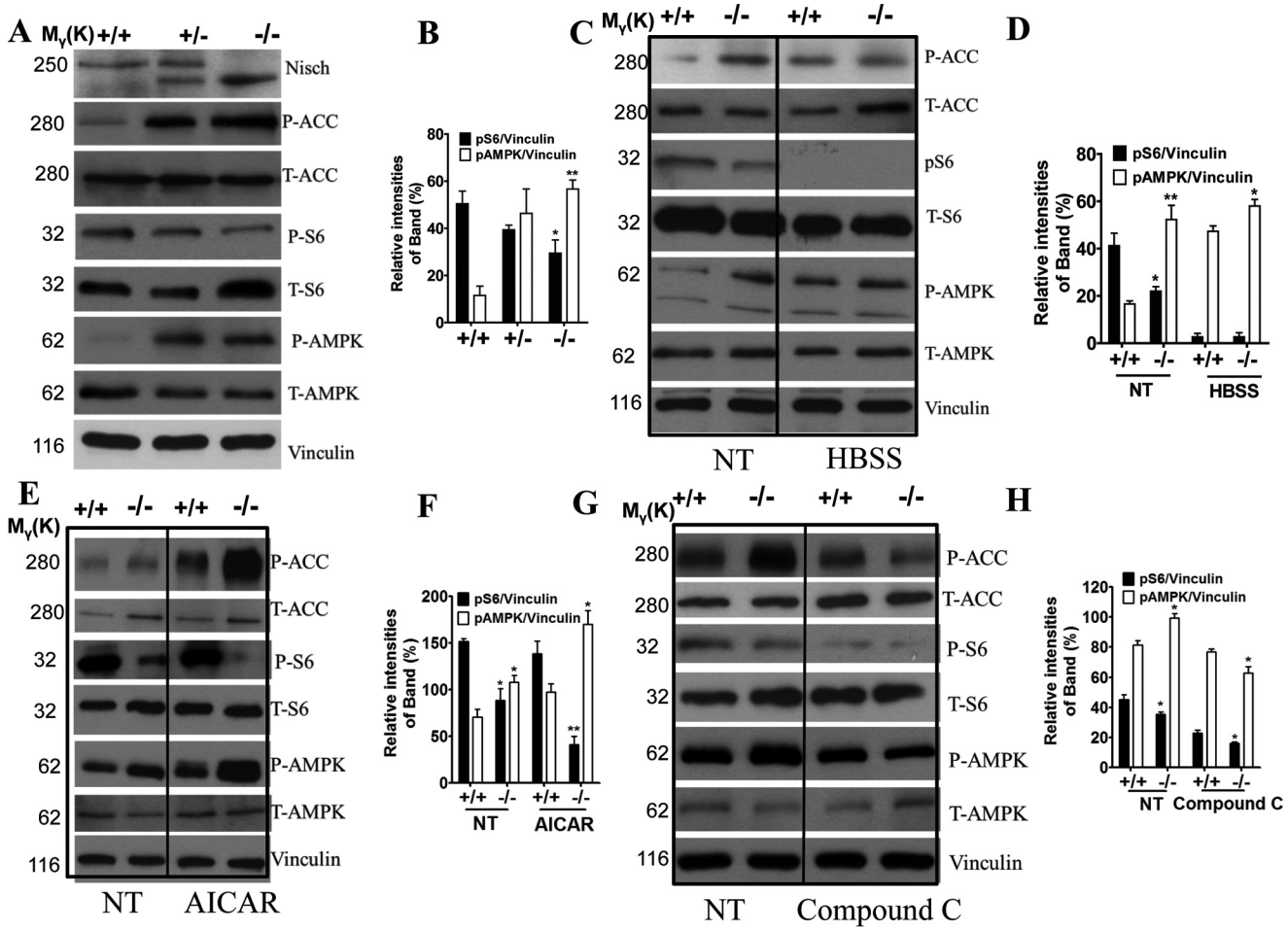

Figure 5. LRR mutation of Nischarin affects AMPK signaling in MEF cells. *A,* lysates were made from WT, Het, and mutant of LRR-mutation MEF cells and subjected to immunoblotting with anti-Nischarin, anti-ACC, anti-phospho-Ser-79-ACC (*P-ACC*), anti-phospho-Ser-235/236-S6 (*P-S6*), anti-S6, anti-phospho-Thr-172-AMPK (*P-AMPK*), and anti-AMPK. Vinculin was used as a loading control. *C,* WT and mutant MEF cell response to nutrient deprivation. After MEFs were seeded in 6-well plates at a density of 200,000 cells/well with complete DMEM for 16 h, the indicated samples were supplied with fresh DMEM containing 10% serum (*NT*) or Hanks' balanced salt solution (*HBSS*) for 4 h. *E,* LRR-deleted MEFs are hypersensitive to pharmacological manipulation of AMPK signaling using AICAR. *G,* LRR-deleted MEFs are hypersensitive to pharmacological manipulation of AMPK signaling using compound C. MEFs were seeded in 6-well plates at a density of 200,000 cells/well and supplied with complete DMEM for 16 h, at which point, the medium was replaced with fresh media (DMEM containing 10% serum) containing either 2 mM AICAR for 2 h or 20 μM compound C for 4 h. *B, D, F,* and *H,* graphical presentation shows the relative abundances of the phosphorylated form of AMPK and S6 shown as percentages of the control in experiments of *A, C, E,* and *G*, respectively. Quantification of band densities was analyzed with ImageJ system (National Institutes of Health, Bethesda) and normalized against vinculin. The data represent the means ± S.E. of three independent experiments. *, $p < 0.05$; **, $p < 0.01$.

discussed previously, AMPK is a key metabolic sensor of cellular energy homeostasis (8). In addition to being regulated by the cellular ATP:AMP ratio, however, AMPK activity is also controlled by phosphorylation, which is catalyzed by several regulatory kinases. LKB1, for example, is a major upstream serine/threonine kinase regulator of AMPK (8). We have recently shown that Nischarin interacts with LKB1 through its integrin-binding domain (7). Similarly, our current findings suggest that Nischarin interacts with AMPK through its LRR domain, resulting in inhibition of AMPK phosphorylation (Fig. 4). Therefore, we explored to what extent Nischarin affects AMPK signaling. We found that Nischarin overexpression resulted in lower AMPK activity in HEK 293T cells (supplemental Fig. 5*D*). In contrast, Nischarin knockdown resulted in higher AMPK activity in PC12 cells (supplemental Fig. 5*E*). Mutant MEFs (+/− and −/−) showed higher AMPK activity as evidenced by the presence of higher levels of Thr-172-phosphorylated AMPK compared with WT MEFs (Fig. 5, *A* and *B*). In addition, Ser-79 phosphorylation of acetyl-CoA carboxylase (ACC), a critical AMPK downstream substrate (8), was also higher in mutant MEFs (Fig. 5*A*). We also assessed the activity of the mammalian target of rapamycin (mTOR)-signaling pathway, which is suppressed in response to AMPK activation. Specifically, we examined S6 and phospho-S6 (Ser-235), two well characterized mTOR signaling components (8). Consistent with the higher AMPK activity in mutant MEFs, we observed lower mTOR activity in mutant MEFs, as evidenced by lower levels of phosphorylated Ser-235 of S6 (Fig. 5, *A* and *B*). These results suggest that Nischarin plays an important role in AMPK–mTOR signaling pathways.

Nischarin LRRs-deletion enhances sensitivity to AMPK activators and inhibitors in MEFs

Given AMPK's crucial importance in glucose metabolism (18), we examined the effect of glucose deprivation and serum starvation using the wild-type and mutant MEFs. We wished to

examine the effects of stress on AMPK signaling in wild-type and mutant MEFs to determine whether AMPK signaling responds in a similar fashion as when altered using AMPK-acting compounds. Following the starvation, we observed an increase in AMPK activity in WT but not in mutant MEFs for reasons that remain unclear. Consistent with this, we did not observe any changes in downstream effectors of AMPK (Fig. 5, *C* and *D*). AICAR is an AMP analog that activates AMPK (19). Mutant MEFs were more sensitive to treatment with 2 mM AICAR than wild-type MEFs, as evidenced by the greater induction of phospho-AMPK (Fig. 5, *E* and *F*). Consistent with this finding, phosphorylated ACC levels also displayed a more robust increase in the mutant MEFs, whereas phosphorylated S6 (S-235) levels were correspondingly decreased (Fig. 5, *E* and *F*). We also inhibited AMPK activity in MEFs using compound C, a direct AMPK inhibitor (20). Once again, the Nisch-mutant MEFs demonstrated greater sensitivity than the non-mutant MEFs, as evidenced by a decrease in phospho-ACC and by increase in phospho-S6 (Fig. 5, *G* and *H*). These data suggest that mutant MEFs were more sensitive to AMPK activators and inhibitors than the wild-type MEFs.

Effects of Nischarin LRR-deletion on AMPK activity in mouse liver and skeletal muscle

We wished to further investigate the role of Nischarin *in vivo*, particularly in tissues crucial for metabolic homeostasis, including liver and skeletal muscle. In mammals, AMPK signals in the hypothalamus, liver, and skeletal muscle regulate food intake, glucose uptake, gluconeogenesis, and fatty acid synthesis and oxidation (21). Thus, we hypothesized that growth defects in Nischarin-mutant mice could likely be due to the disturbance in normal metabolism following AMPK activation. Consistent with the results in MEFs, Nischarin mutation in the liver of 1-month-old mice increased AMPK phosphorylation at Thr-172 (Fig. 6, *A* and *C*). The higher AMPK activity was also accompanied by an increased Ser-79 phosphorylation of ACC and decreased Ser-235 phosphorylation of S6 in liver (Fig. 6, *A* and *C*). Overnight fasting resulted in an increase in the phosphorylation of AMPK in wild-type liver (Fig. 6*A*) without an increase in the phosphorylation of ACC and S6 in wild-type liver. Although overnight fasting did not change the phosphorylation of AMPK in the liver of Nischarin-mutant mice, the phosphorylation of ACC was abolished, and mTOR signaling was stimulated (Fig. 6*A*).

We next investigated AMPK activation in skeletal muscle of Nischarin-mutant mice. In 1-month-old male mice, Nischarin mutation resulted in an increase of AMPK activity in the skeletal muscle, which was accompanied by an increased phosphorylation of ACC and decreased phosphorylation of S6 (Fig. 6, *B* and *D*). We did not observe a significant effect of overnight fasting on the AMPK signaling in skeletal muscle of wild-type mice. However, overnight fasting resulted in a significant increase on the phosphorylation of AMPK in the skeletal muscle of Nischarin-mutant mice (Fig. 6*B*). Similar results were also observed in the liver and skeletal muscle of 3-month-old male mice (data not shown).

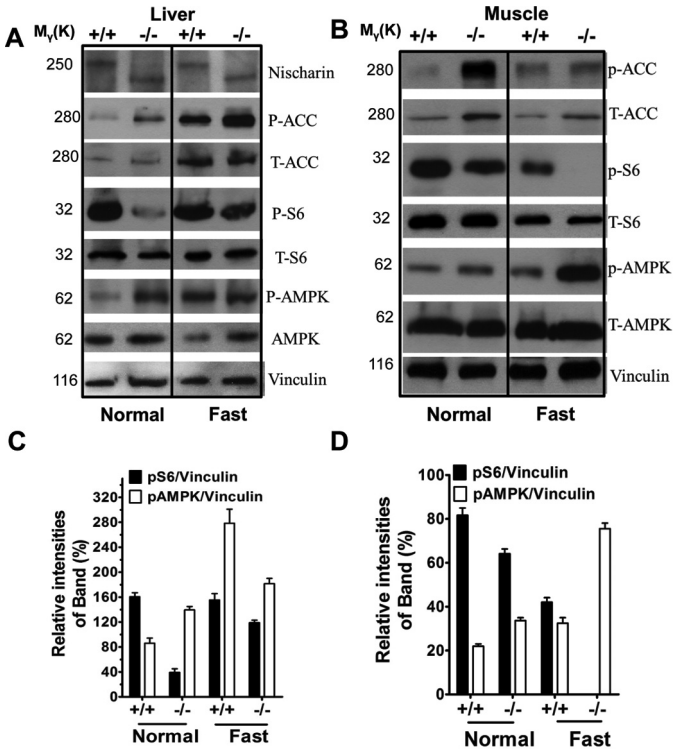

Figure 6. LRR mutation of Nischarin affects AMPK signaling in liver and muscle tissues. *A* and *B*, immunoblotting of liver protein lysates (*A*) and muscle protein lysates (*B*) with indicated antibodies. One-month-old mice of indicated genotypes were fasted for 16 h or fed *ad libitum* (normal) and then sacrificed using CO_2. Liver and muscle (hind limb) were immediately collected and snap-frozen in liquid nitrogen. Proteins from total cell extracts of liver or muscle were immunoblotted for proteins in AMPK signaling. *C* and *D*, Western blots were quantified by densitometry as percentages of the control in the experiments of *A* and *B*, respectively. Quantification of the phosphorylated AMPK and S6 band densities was analyzed with ImageJ system (National Institutes of Health, Bethesda) and normalized against vinculin. The data represent the mean ± S.E. of three independent experiments.

Nischarin LRR-deletion decreases lipogenic and gluconeogenic gene expression in the liver and muscle

To explore the consequence of increased AMPK activation in muscle and liver, we quantified the expression levels of critical lipogenic genes by qRT-PCR. Activation of AMPK promotes inhibitory phosphorylation of ACC. It has also been shown that fatty-acid synthase (FAS) expression is reduced in response to AMPK activation. Consistent with these reports, Nischarin mutation reduced FAS (Fig. 7, *A* and *C*). Activation of AMPK has previously been shown to alter the function of lipogenic genes, including sterol regulatory element-binding protein-1 (SREBP1c) and the carbohydrate-response element-binding protein (ChREBP) (22, 23). The expression of SREBP1c and ChREBP mRNA was reduced in Nischarin mutant liver and muscle tissues (Fig. 7, *B* and *D*). In short, Nischarin-mutated tissues showed reduced gene expression of lipogenic enzymes. We also examined the expression of several critical gluconeogenic genes, including glucose-6-phosphatase and peroxisome proliferator-activated receptor-γ co-activator 1α (PGC1α), in mouse liver and skeletal muscle. Glc-6-Pase hydrolyzes glucose 6-phosphate, yielding a phosphate group and a free molecule of glucose, which can then be exported from the cell. Consistent with previous observations that activation of AMPK (*e.g.* using metformin, an AMPK-activating drug) leads to suppression of

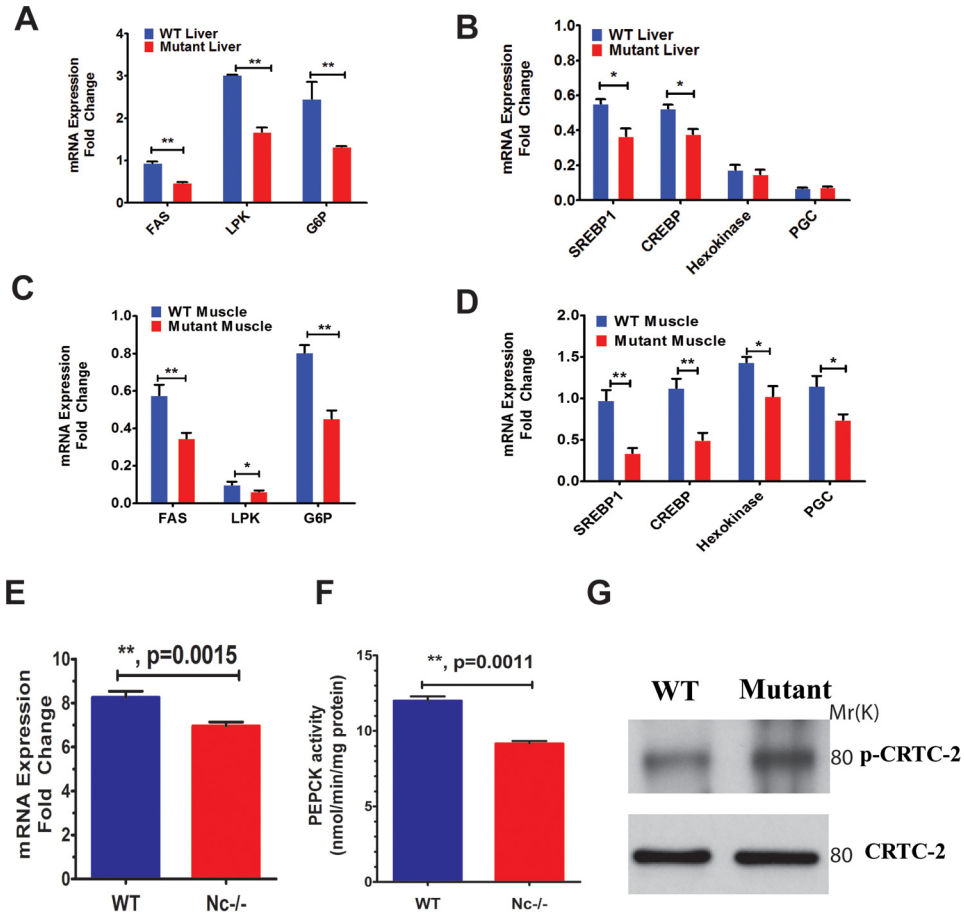

Figure 7. Gluconeogenic and lipogenic gene expression is down-regulated in the liver and muscle of Nischarin LRR-mutation mice. *A–D*, qRT-PCR for FAS, L-PK, Glc-6-P (*G6P*), SREBP1, ChREBP, hexokinase, and PGC genes in the liver (*A* and *B*) and muscle (*C* and *D*) tissue of 1-month-old WT and mutant mice. Expression was normalized to β-actin. qRT-PCR data represent the mean ± S.E. Samples were analyzed at least in triplicate. *, $p < 0.05$; **, $p < 0.01$. *E*, PEPCK mRNA expression by qRT-PCR in liver samples collected from 2-month-old mice. *F*, effects of LRR mutation on PEPCK activity in 2-month-old mouse liver samples. *G*, LR mutation increases CRTC2 phosphorylation in mutant MEFs The data represent three independent experiments.

Glc-6-Pase (24, 25), we found that Nischarin mutation could also lead to reduced expression of Glc-6-Pase (Fig. 7, *A* and *C*). Hexokinase (HK), which converts glucose into Glc-6-P, plays a pivotal role in glycolysis. It has previously been shown that metformin inhibits HK possibly by up-regulation of AMPK (26). In agreement with this, we found that Nischarin mutation similarly inhibits HK expression in the muscle (Fig. 7*D*). For reasons unknown, HK and PGC1α expression did not change in the liver; however, they are down-regulated in Nischarin mutant muscle tissue. Although several previous reports indicate that PGC1α expression is enhanced upon AMPK activation (27), our data indicate that Nischarin mutant livers (which exhibit higher levels of AMPK) show decreased PGC1α. The final glycolytic enzyme, which we found to be altered in Nischarin-mutant mice, was liver pyruvate kinase (L-PK), which catalyzes phosphoenolpyruvate to yield pyruvate and ATP. Consistent with previous reports (28), we observed a reduction in L-PK expression in Nisch-mutant livers and only a modest change in the muscle (Fig. 7, *A* and *C*). Given our findings that Nischarin inactivation results in reduced expression of Glc-6-Pase, we investigated whether other gluconeogenic enzymes might similarly be affected (29). Interestingly, we found that PEPCK, which catalyzes the initial step of gluconeogenesis, was altered in Nischarin-mutant mice as well. Like Glc-6-Pase, the gene expression of PEPCK was reduced in Nischarin-mutant liver (Fig. 7*E*) and muscle (supplemental Fig. 8). In addition, we also observed a decrease in the activity of the enzyme as well (Fig. 7*F*). These data suggest that Nischarin mutation inhibits PEPCK leading to inhibition of gluconeogenesis, and thus they are more tolerant to glucose and display a smaller, leaner body type. In the liver, activation of AMPK suppresses hepatic gluconeogenesis by phosphorylation of several targets, including CREB-binding protein, CREB-regulated transcription co-activator (CRTC2), and glucose synthase kinase b (GSK3b) (29–31). To evaluate whether the reduced expression of Glc-6-Pase and PEPCK could have resulted from the inhibition of these regulators, we investigated whether they also showed differential expression between Nischarin mutant and wild-type mice. As expected, CRTC2 phosphorylation is dramatically increased in Nisch-mutant livers (Fig. 7*G*) further suggesting that Nischarin mutation inhibits hepatic gluconeogenesis.

Ablation of Nischarin affects glucose uptake

We have previously reported that Nisch inhibits cell migration; thus, we wished to corroborate this using our LRR-domain deletion MEF cell model. Consistent with our previous data, mutant MEFs showed enhanced motility compared with the wild-type MEFs (supplemental Fig. 9*A*). Because Nisch appears

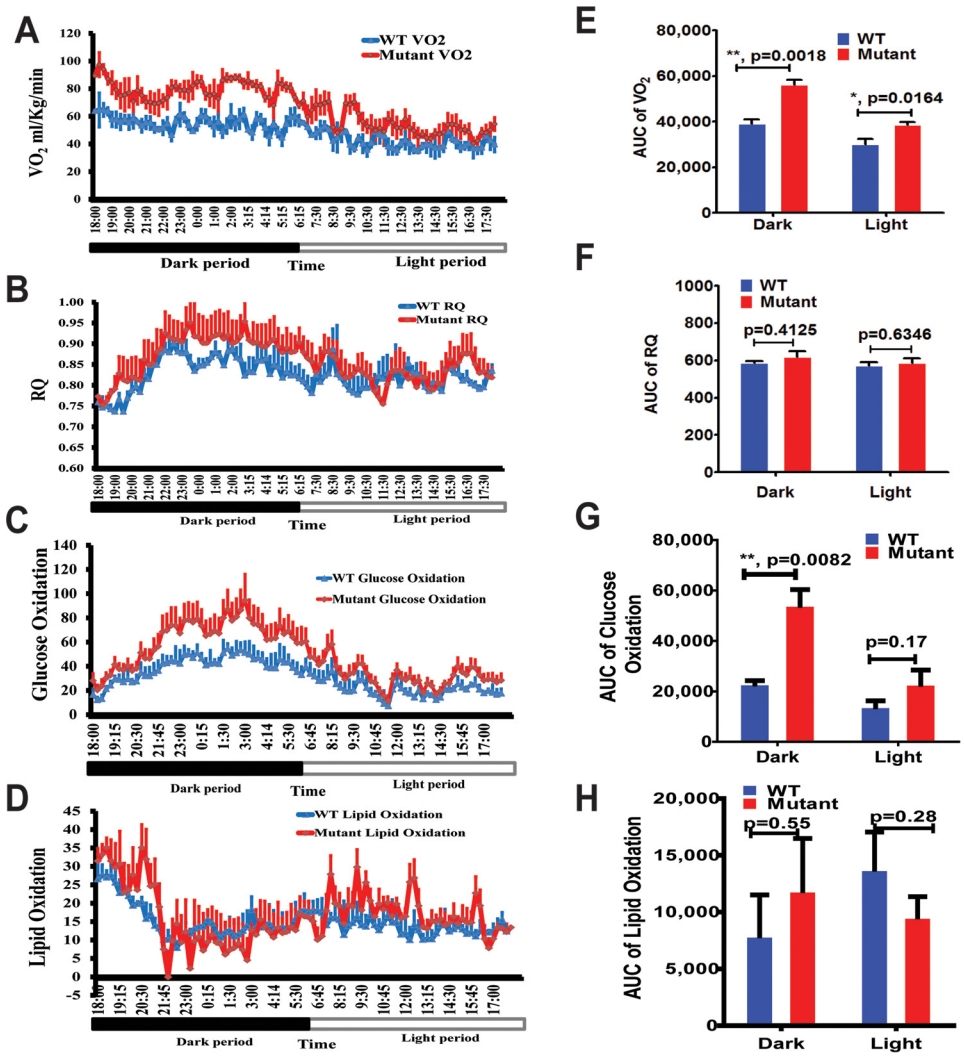

Figure 8. Nischarin LRR mutation elevates the mouse oxygen consumption and glucose oxidation. Oxygen consumption (VO_2) (*A*) and RQ (*B*) were measured in air-tight chamber for age-matched WT ($n = 3$) *versus* mutant ($n = 4$) male mice. *C* and *D*, glucose (*C*) and lipid oxidation (*D*). *E–H,* AUC values for the dark and light periods of *A–D*, respectively. Data represent the mean ± S.E. *, $p < 0.05$; **, $p < 0.01$; ***, $p < 0.0001$.

to play an important role in cellular glucose uptake, we also tested whether LRR-domain deletion affects glucose uptake; we incubated wild-type, Het, and mutant MEFs with 2-NBDG, a fluorescent derivative of glucose that can be detected by FACS assay. Wild-type and Het MEFs produced two peaks during 2-NBDG measurement, in which the lower peak indicated the cell population with low 2-NBDG uptake and the higher peak for the cell population with high 2-NBDG uptake. Mutant MEFs absorbed less 2-NBDG compared with the wild-type MEFs and failed to produce a peak corresponding to a high 2-NBDG uptake population (supplemental Fig. 9*B*). These data indicate that mutation of the LRR domain inhibits glucose uptake suggesting that Nischarin plays an important role in glucose uptake, and the LRR domain is critical for this function.

Next, we analyzed oxygen consumption and respiratory quotient (RQ) of Nisch-mutant animals by indirect calorimetry (32). Using 24-h indirect calorimetry, we examined changes in basal metabolism. Nischarin-mutant mice exhibited increased oxygen consumption, RQ, and heat production for both light and dark cycles (Fig. 8, *A–D,* and *F–H*; supplemental Fig. 10). It is likely higher glucose oxidation rate in Nischarin-mutant mice compared with the WT animals (Fig. 8, *C* and *H*) leading to increased heat production (supplemental Fig. 10, *B* and *D*); however, the data are significant and thus inconclusive. Similarly, lipid oxidation data are not significant. The augmented RQ increased whole-body utilization of glucose and protein for energy.

Real-time analysis of bioenergetic pathways in MEF cells

The total cellular ATP content is affected by ATP production from glycolysis and ATP consumption by mitochondrial oxidative phosphorylation (33). Thus, we analyzed mitochondrial oxidative phosphorylation by measuring the oxygen consumption rates (OCR) on an XF24 Extracellular Flux Analyzer. The basal oxygen consumption rate was unchanged in mutant MEFs; however, oxygen consumption was higher in mutant MEFs than in wild-type MEFs when mitochondrial oxidative phosphorylation was blocked by FCCP, which uncouples the mitochondrial proton gradient (supplemental Fig. 11). The extracellular acidification rate (ECAR) remained unchanged (data not shown).

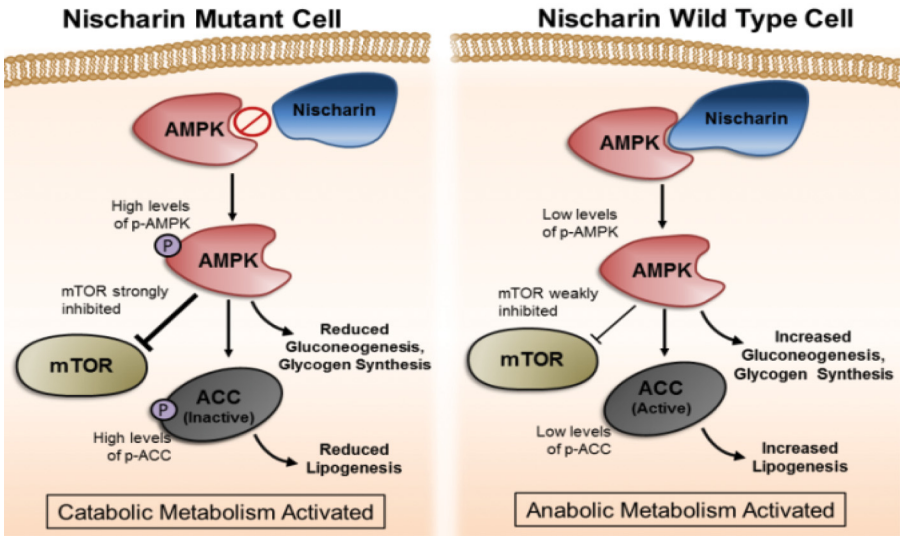

Figure 9. Schematic illustrating the effect of Nischarin mutation on AMPK signaling. AMPK activity is inversely related to the degree of interaction between AMPK and Nischarin. The downstream mediators include ACC as well as mTOR, which are comparatively more active when wild-type Nischarin is present but show reduced activity in Nischarin mutant cells.

Discussion

The chief finding of this study is that Nischarin binds and inhibits AMPK, which implicates Nisch as a modulator of both metabolic and physiological processes beyond its traditional role as a tumor suppressor. To achieve tumor suppression, Nischarin interacts with multiple proteins, notably LKB1 (7). Because AMPK is a downstream effector of LKB1 (8), we examined the levels of active LKB1 but found no apparent changes in Nischarin mutant animal cells (data not shown), indicating that Nischarin's effects on AMPK are likely independent of its interaction with LKB1.

Because the LRR domain in Nischarin is predicted to play an important role in protein interactions (10–12), we deleted this region in Nischarin-mutant mice. The results indicated that the interactions between mutant Nischarin and its binding partners were defective, supporting our assertion that this particular region is important for Nischarin–AMPK interaction. This relationship and its consequences are illustrated in Fig. 9, which summarizes the key alterations in metabolic signaling pathways that occur in the presence or absence of mutant Nischarin. As indicated, the level of active (phosphorylated) AMPK is inversely related to the degree of interaction between AMPK and Nischarin. The chief downstream mediators responsible for the effects of Nischarin regulation include ACC as well as mTOR, which are comparatively more active when wild-type Nischarin is present, but they show reduced activity in Nischarin mutant cells, leading to the preference toward catabolic pathways exhibited by these cells. When taken together, the evidence reported here has led us to the conclusion that Nischarin physically interacts with AMPK to inhibit AMPK functions and that a full-length Nischarin is necessary for this interaction to take place. Binding of Nischarin to AMPK may keep AMPK inhibited, and thus, in Nischarin LRR-deleted cells, the weakened affinity between them enhances AMPK activation.

Nischarin is also known as imidazoline receptor antiserum-selected (IRAS) (34). The mouse *nisch* gene contains 21 exons and spans 46 kb. Zhang *et al.* (35) generated IRAS mutant mice by deleting 49-bp-long exon 4. Interestingly, their IRAS mutant mice shared a similar growth-retarded phenotype as our Nischarin LRR-deletion mice. Although there were no functional motifs in exon 4, they were able to see the same effect as we observed (35). Thus, further characterization of these mice is essential to connect their phenotype to the changes in metabolism and signaling pathways.

Nischarin's functions suggest that it is a scaffolding protein. This conclusion is supported by the comparative similarity of its characteristics to those of other known scaffolding proteins, such as IQGAP1. A well-studied and prototypical scaffolding protein, IQGAP, interacts with at least 100 different proteins and plays role in multiple signaling pathways that regulate various biological processes (36, 37). Similar to IQGAP1, Nischarin affects actin polymerization and localizes near the leading edge of lamellipodia (4, 38). IQGAP1 interacts with Ras, Raf, MEK, and ERK in the same signaling cascade (39); similarly, Nischarin interacts with Rac, PAK, and LIMK in the same signaling cascade (2). Although Nischarin is not a transcription factor, it does regulate expression of α5 integrin (3), possibly through association with other protein(s). Similarly, IQGAP1 regulates transcription through its association with Yes-associated protein (40). More recently, the IQGAP1 protein has also been implicated in insulin resistance (41). Because scaffold proteins interact with many binding partners, it is possible that multiple signaling pathways are interconnected or the scaffold proteins have independent functions in different systems and organs. For instance, IQGAP1 plays an important role in kidney through its association with nephrin protein (42), whereas IQGAP1 regulates insulin secretion through its association with exocyst complex (43) or Rab27a (44). Interestingly, IQGAP1 interacts with AMPK as well (36, 37). In summary, it is hard to determine the exact signaling mechanism of a scaffold protein in an organ or disease, due to the sheer number of protein interactions that they typically host. Thus, the mechanism we propose here represents merely one way by which Nischarin regulates animal growth and development

From a therapeutic point of view, inhibition of Nischarin function may have beneficial effects in preventing the progression of metabolic disorders, such as type 2 diabetes and obesity, because high levels of AMPK activity support glucose oxidation (45) and inhibit lipogenesis (22). Therefore, targeting Nischarin function theoretically could be employed to enhance AMPK activity, thus improving metabolic function. In addition, given that mutant Nisch cells were found to be more sensitive to AICAR and compound C compared with WT cells, the use of a combination of compounds (which inhibits Nischarin while simultaneously enhancing AMPK) could offer synergistic results, leading to greater efficacy than use of either one alone.

To monitor the effect of Nisch abrogation, we examined AMPKα subunit phosphorylation in tissues from Nisch-mutant animals and found that AMPKα subunit phosphorylation was higher in Nisch-mutant MEFs, liver, and skeletal muscle. It has been shown that activation of AMPK inhibits hepatic lipid accumulation by inhibiting lipogenesis (46). Consistent with this, our data show that Nischarin mutation inhibits several lipogenic genes, including ACC, FAS, and SREBP1c, a master regulator of *de novo* lipogenesis (47). Because Nischarin mutation suppresses SREBP1c expression, it is likely that Nischarin plays a role in cholesterol metabolism in addition to regulating fatty acid synthesis. In addition, Nischarin mutation resulted in decreased expression of genes involved in gluconeogenesis such as HK, Glc-6-Pase, PGC1α, and ChREBP. Importantly, the CRTC2 transcription factor is a CREB and major regulator of glucose metabolism. It has been suggested that CREB–CRTC2 activity is critical for the maintenance of glucose homeostasis (48). CRTC has been shown to be phosphorylated at Ser-171 by AMPK and relocated from the nucleus to cytosol, preventing CREB-regulated genes, such as PEPCK and Glc-6-Pase, from being activated. Thus, our findings support the notion that Nischarin mutation leads to the promotion of catabolism in a tandem fashion: first by reducing the activity of enzymes directly involved in biosynthesis (*e.g.* ACC) (49), and second by altering the expression of several other genes (*e.g.* SREBP1c and ChREBP) involved in regulating metabolism (50). Consistent with increased AMPK activation, Nischarin mutation enhanced energy balance with increased glucose oxidation and energy expenditure, as well as suppressed food intake. Although Nisch-mutant mice exhibited enhanced glucose tolerance, insulin tolerance was comparable with that in WT animals. In summary, our data reveal a novel role for Nischarin as an key inhibitor of AMPK activity and an important regulator of cellular energy balance and lipid and glucose metabolism.

Experimental procedures

Antibodies and chemicals

Anti-phospho-AMPK (Thr-172), anti-phospho-ACC (Ser-79), anti-ribosomal protein S6, anti-ACC, anti-AMPK, and anti-LKB1 antibodies were obtained from Cell Signaling Technology (Beverly, MA). Anti-phospho-ribosomal protein S6 (Ser-235/236) and anti-phospho-LKB1 were purchased from Santa Cruz Biotechnology (Santa Cruz, CA). Anti-vinculin was purchased from Sigma. Mouse anti-Nischarin antibody was from BD Biosciences. CRTC2 and p-CRTC2 were kindly provided by Dr. Hiroshi Takemori (National Institute of Biomedical Innovation, Japan). Secondary anti-mouse IgG with horseradish peroxidase was from Calbiochem. Secondary anti-rabbit IgG with horseradish peroxidase was from GE Healthcare. Metformin was purchased from MP Biomedicals. AICAR was from AdipoGen. Rapamycin was from LC Laboratories. 2-NBDG was from Invitrogen.

Co-immunoprecipitation

For Nischarin–AMPK interaction experiments, 293T cells were transiently transfected with 4 μg each of FLAG–AMPKα2 (kindly provided by Dr. Hong-Gang Wang, Department of Pharmacology, Pennsylvania State University), Myc–Nischarin deletion constructs, and full-length Myc–Nischarin using Lipofectamine 2000 (Invitrogen) transfection reagent. Forty eight hours later, the cells were lysed in FLAG lysis buffer with protease inhibitors. The clarified lysates were incubated overnight with mouse anti-FLAG M2, or rat anti-FLAG, or mouse anti-Myc antibodies at 4 °C in combination with protein G-Sepharose (GE Healthcare). The co-immunoprecipitated proteins were detected by primary anti-Myc or anti-FLAG antibodies overnight at 4 °C. The secondary mouse antibodies were blotted for 1 h at room temperature. The horseradish peroxidase activity was visualized with Super-Signal West Pico Chemiluminescent substrate (Pierce).

For endogenous co-immunoprecipitation, PC12 lysates were subjected to immunoprecipitation with mouse anti-Nischarin antibody (sc-374407, Santa Cruz Biotechnology) or control mouse IgG antibody, followed by Western blot analyses with anti-Nischarin and anti-AMPK α1/2 antibodies (Bethyl Laboratories). The freshly isolated WT and Nischarin null mice liver were snap-frozen in liquid nitrogen. Liver protein extracts were prepared by grinding tissue into a fine powder in liquid nitrogen and subsequently dissolving in FLAG lysis buffer supplemented with protease inhibitor and phosphatase inhibitors. The lysates were centrifuged at 13,000 rpm for 15 min, and the supernatant was collected as extracted protein. Protein concentrations were determined using a BCA protein assay. The liver extracts were subjected to immunoprecipitation with rabbit anti-Nischarin antibody or control IgG antibody, followed by Western blot analyses with anti-Nischarin and anti-AMPK antibodies (sc-74461, Santa Cruz Biotechnology).

Nutrient starvation and drug treatments for MEF cells

MEF cells were seeded onto 6-well plates at a density of 200,000 cells per well. After culturing in complete DMEM for 16 h, media were replaced with fresh DMEM containing 10% FBS and 2 mM AICAR for 2 h, DMEM with 10% FBS and 20 μM compound C for 4 h, or Hanks' balanced solution for 3 h after three separate washes. In control cells, media were replaced with fresh DMEM with 10% FBS. Cells were lysed in radioimmunoprecipitation (RIPA) lysis buffer with protease inhibitor mixture (Roche Applied Science), and phosphatase inhibitors after the experiments were executed. Protein concentrations were determined using a bicinchoninic acid (BCA) protein assay (Thermo Fisher Scientific, Waltham, MA). Samples were

boiled in SDS sample buffer for 15 min and stored at −80 °C until analysis.

Liver and muscle tissue protein analysis

Wild-type and mutant male mice (1 and 3 months old) were provided with normal food or fasted overnight. After each experiment, liver and skeletal muscle (hind limb) samples were snap-frozen in liquid nitrogen and stored at −80 °C until further analysis. Liver or muscle protein extracts were prepared by grinding tissue into a fine powder in liquid nitrogen and subsequently dissolving in RIPA buffer supplemented with complete protease inhibitor mixture tablet (Roche Applied Science) and phosphatase inhibitors. The lysates were centrifuged at 13,000 rpm for 15 min, and the supernatant was collected prior to protein extraction. Protein concentrations were determined using a bicinchoninic acid (BCA) protein assay (Thermo Fisher Scientific). An equal amount of protein lysates was separated by SDS-PAGE and then transferred to a PVDF membrane and detected with various antibodies.

Glucose uptake assay

To measure glucose uptake, 5×10^5 MEF cells were incubated in 37 °C water bath for 2 h with 1 ml of PBS containing 100 μM 2-NBDG (Invitrogen). The 2-NBDG uptake reaction was stopped by washing the cells with pre-cold PBS. Cells were resuspended in 0.5 ml of ice-cold PBS with 2% FBS. Fluorescence intensity from 10,000 single-cell events was obtained using a FACSCalibur flow cytometer (BD Biosciences). Data were analyzed using FlowJo software.

Seahorse XF-24 metabolic flux analysis

OCR and ECAR in WT, Het, and mutant MEFs were measured at 37 °C using the Seahorse 24XF instrument (Seahorse Biosciences, North Billerica, MA) following the manufacturer's protocols. MEFs were seeded in a Seahorse 24-well tissue culture plate at a density of 40,000 cells per well for 16 h. Cells were then changed to unbuffered XF assay media at pH 7.4 (Seahorse Biosciences) supplemented with 25 mM glucose (Sigma) and 1 mM sodium pyruvate (Invitrogen). Prior to performing the Seahorse measurements, cells were incubated for 1 h at 37 °C in a non-CO_2 incubator. Respiration was measured before and after the injection of three compounds: oligomycin (1.5 μM) injection 1, FCCP (2.5 μM) at injection 2, and rotenone (1 μM) at injection 3. All injection reagents were adjusted to pH 7.4 on the day of the assay. Experiments were performed in real time in 6–7 replicate wells for each MEF strain. OCR and ECAR were automatically calculated by the Seahorse XF-24 software. Immediately after the completion of the measurements, cells were trypsinized and counted to normalize individual well-rate data to cell counts.

Histological examination

Embryos at day 18.5 were isolated, genotyped, and fixed in 4% paraformaldehyde. Fixed embryos were rinsed with PBS, paraffin-embedded, and sectioned. Sections were stained by hematoxylin and eosin.

Liver and muscle tissue RNA extractions

Wild-type and mutant male mice (1 and 3 months old) were given normal food or fasted overnight. After each experiment, liver and skeletal muscles (hind limb) samples were soaked in RNAlater solution (Ambion) and stored at −80 °C until analysis. Liver tissues were ground into a fine powder in liquid nitrogen, and subsequently RNAs were extracted using RNeasy Plus mini kit according to the manufacturer's protocol. After muscle tissues were ground into a fine powder in liquid nitrogen and dissolved in RVL plus buffer, proteinase K (final concentration of 10 mg/ml) was added, and samples were incubated at 55 °C for 30 min. Subsequently, RNA extraction followed manufacturer's protocol using RNeasy Plus mini kit.

Glucose tolerance and insulin tolerance tests

Blood glucose levels were measured using Abbott AlphaTrak blood glucose monitoring system, which is minimally invasive and gives rapid and reliable results. We performed an intraperitoneal injection glucose-tolerance test. Prior to glucose administration, mice were fasted for 16 h to achieve a baseline blood glucose level. After fasting, mice were administered glucose (2 g/kg) by intraperitoneal injection. A 2-mm distal section of each mouse's sterilized tail was snipped using a scalpel and gently squeezed to obtain two drops of blood, the first of which was discarded. The second drop was applied directly to an AlphaTrak glucometer test strip to obtain a baseline of blood glucose reading. The fasted mice were then given D-glucose (2 mg/g of body weight) by i.p. injection. Blood samples were taken at 15, 30, 60, 90, and 120 min after glucose administration. The insulin tolerance test protocol was identical to the glucose tolerance test except that mice first underwent a 6-h fast. Human insulin diluted in sterile water was administered by i.p. injection in lieu of glucose administration at 0.75 units/kg. Blood glucose levels were monitored as above immediately prior to injection t_0 and at 30, 60, 90, and 120 min after injection.

RNA extraction from organs

Mice were fed *ad libitum* and then sacrificed using CO_2. Liver and muscle (hind limb) were immediately collected and snap-frozen in liquid nitrogen. 100-milligram tissue specimens were ground into fine powder using mortar and pestle in liquid nitrogen. Total RNA was isolated using TRIzol reagent. The potential contaminated DNA were removed by DNase I digestion.

Quantitative RT-PCR analysis

RT-PCR was performed with 700 ng of total RNA using the Multiscribe reverse transcriptase (High-Capacity cDNA archive kit, Applied Biosystems, Foster City, CA) following the manufacturer's instructions. The cDNA was diluted 1:4 in nuclease-free water. The real time PCR contained 2.5 μl of 2× SYBR Green PCR Master Mix, 0.2 μM forward and reverse primers (final concentration), 1 μl of cDNA, and water up to 5.0 μl. Primer sets used are indicated in supplemental Table 1. The PCR was performed in a QuantStudio system (Life Technologies, Inc.). All reactions were performed in triplicate. The

expression level was analyzed using the $2^{-\Delta\Delta Ct}$ method (51). β-Actin was used as the endogenous control gene, and a pool of all of the cDNA samples was used as the calibrator. The results are shown as fold change of the expression level relative to the housekeeping gene. Data are shown as means ± S.D. Statistical analysis was performed in Microsoft Excel (Microsoft Corp., Redmond, WA).

PEPCK assay

Freshly isolated liver and muscle tissues from 2-month-old mice were minced and homogenized using a PowerGen 125 homogenizer (Thermo Fisher Scientific) in homogenization buffer, which contains 300 mM sucrose, 1 mM EDTA, 0.5% fatty acid-free BSA, 1 mM DTT, 1 mM PMSF, and 10 mM Tris-Cl, pH 8.0. Homogenates were then sonicated with three 5-s pulses on ice and centrifuged at 15,000 × *g* for 10 min at 4 °C. Protein concentrations in the supernatants were determined using a BCA protein assay kit (Thermo Fisher Scientific). The lysates were then aliquoted and stored at −80 °C until use. A malate dehydrogenase-coupled enzymatic assay was used to measure PEPCK activity as described (52, 53). The reactions were performed in triplicate with a final volume of 500 μl containing 50 mM HEPES, pH 6.5, 3 mM $MnCl_2$, 3 mM $MgSO_4$, 13 mM NaF, 1 μM rotenone, 45 mM $NaHCO_3$, 0.15 mM NADH, 6 units/ml malate dehydrogenase, 2 mM phosphoenolpyruvate in 48-well plates. After incubation at 30 °C for 2 min, the reaction was initiated with 0.5 mM dGDP. The oxidation of NADH by malate dehydrogenase was measured at 340 nm using a microplate spectrophotometer (Benchmark Plus, Bio-Rad). Control samples lacking $NaHCO_3$ were run simultaneously, and this background was subtracted in reactions. One unit of PEPCK activity corresponds to the production of 1 μmol of product min^{-1} at 30 °C.

RQ measurement

We used adult (5 months old) male WT ($n = 3$) and mutant ($n = 4$) C57BL6 mice for the whole-body energy metabolism assessment by indirect calorimetry, which was performed using a PhysioScan Metabolic System (Omnitech Electronics, Columbus, OH). The system consists of a single metabolic chamber, CO_2 and O_2 analyzers, and electronic flow regulators. Output parameters include CO_2 production (VCO_2, ml/kg/min), O_2 consumption (VO_2, ml/kg/min), RQ (VCO_2/VO_2), and heat production (calories/h). A mouse was placed into an airtight chamber (8 inches long × 8 inches wide × 5.5 inches high) for the VCO_2 and VO_2 measurement. While in the cage, mice were allowed access to water and diet *ad libitum*, and the animal could move freely. Atmospheric air was drawn into the chamber at a rate of 500 ml/min. Each mouse was monitored at the beginning of the dark phase of the 12-h light and 12-h dark cycle. Although the animals behaved routinely, the VO_2 and VCO_2 were recorded every 5 min. The concentrations of the gases were recorded in ml/kg body weight/min by the machine. The RQ was calculated as follows: $RQ = VCO_2/VO_2$. The measurement was done for one 24-h period. The glucose and lipid oxidation rates were calculated using the equations of Frayn (54), which defines the glucose oxidation (g/min) as 4.55 VCO_2 (liter/min) − 3.21 VO_2 (liter/min) − 2.87*N* (mg/min) and the lipid oxidation (g/min) as 1.67 VCO_2 (liter/min) − 1.67 VO_2 (liter/min) − 1.92*N* (mg/min), where *N* represents the rate of urinary nitrogen excretion used to estimate protein oxidation. Considering the fact that only a small portion of energy expenditure arises from protein oxidation under experimental conditions, the contribution of protein oxidation was neglected. Animals were sacrificed afterward as per protocol. The data were further analyzed in Word Excel. Data represent mean ± S.E.

Statistical analysis

Data are shown as means ± S.E. unless indicated otherwise. A two-tailed unpaired Student's *t* test was applied for statistical analysis to compare the two groups of interest, and $p < 0.05$ was considered statistically significant. Graphical information was performed using GraphPad Prism software (GraphPad Software Inc., San Diego).

Author contributions—S. K. A. and S. D. designed the study. S. D., S. B., A. G., S. S. G., S. E., and T. I. performed the experiments. D. M. helped with statistical analysis and S. K. A. and S. D. interpreted the data. S. K. A. and S. D. wrote the manuscript. F. M. J. helped with metabolism approaches.

Acknowledgments—We thank Dr. Kartik Shankar of University of Arkansas, Little Rock, AR for good discussions on indirect calorimetry and Dr. Dorota Wyczechowska of Louisiana State University Health Science Center (LSUHSC) for help with Seahorse experiments.

References

1. Alahari, S. K., Lee, J. W., and Juliano, R. L. (2000) Nischarin, a novel protein that interacts with the integrin α5 subunit and inhibits cell migration. *J. Cell Biol.* **151,** 1141–1154
2. Maziveyi, M., and Alahari, S. K. (2015) Breast cancer tumor suppressors: a special emphasis on novel protein Nischarin. *Cancer Res.* **75,** 4252–4259
3. Baranwal, S., Wang, Y., Rathinam, R., Lee, J., Jin, L., McGoey, R., Pylayeva, Y., Giancotti, F., Blobe, G. C., and Alahari, S. K. (2011) Molecular characterization of the tumor-suppressive function of Nischarin in breast cancer. *J. Natl. Cancer Inst.* **103,** 1513–1528
4. Alahari, S. K., Reddig, P. J., and Juliano, R. L. (2004) The integrin-binding protein Nischarin regulates cell migration by inhibiting PAK. *EMBO J.* **23,** 2777–2788
5. Ding, Y., Milosavljevic, T., and Alahari, S. K. (2008) Nischarin inhibits LIM kinase to regulate cofilin phosphorylation and cell invasion. *Mol. Cell. Biol.* **28,** 3742–3756
6. Alahari, S. K., and Nasrallah, H. (2004) A membrane proximal region of the integrin α5 subunit is important for its interaction with Nischarin. *Biochem. J.* **377,** 449–457
7. Jain, P., Baranwal, S., Dong, S., Struckhoff, A. P., Worthylake, R. A., and Alahari, S. K. (2013) Integrin-binding protein Nischarin interacts with tumor suppressor liver kinase B1 (LKB1) to regulate cell migration of breast epithelial cells. *J. Biol. Chem.* **288,** 15495–15509
8. Shackelford, D. B., and Shaw, R. J. (2009) The LKB1-AMPK pathway: metabolism and growth control in tumour suppression. *Nat. Rev. Cancer* **9,** 563–575
9. Suzuki, T., Bridges, D., Nakada, D., Skiniotis, G., Morrison, S. J., Lin, J. D., Saltiel, A. R., and Inoki, K. (2013) Inhibition of AMPK catabolic action by GSK3. *Mol. Cell* **50,** 407–419
10. de Wit, J., Hong, W., Luo, L., and Ghosh, A. (2011) Role of leucine-rich repeat proteins in the development and function of neural circuits. *Annu. Rev. Cell Dev. Biol.* **27,** 697–729
11. Jha, S., and Ting, J. P. (2009) Inflammasome-associated nucleotide-binding domain, leucine-rich repeat proteins and inflammatory diseases. *J. Immunol.* **183,** 7623–7629

12. Bella, J., Hindle, K. L., McEwan, P. A., and Lovell, S. C. (2008) The leucine-rich repeat structure. *Cell. Mol. Life Sci.* **65,** 2307–2333
13. Ng, A. C., Eisenberg, J. M., Heath, R. J., Huett, A., Robinson, C. M., Nau, G. J., and Xavier, R. J. (2010) Human leucine-rich repeat proteins: a genome-wide bioinformatic categorization and functional analysis in innate immunity. *Proc. Natl. Acad. Sci. U.S.A.* **108,** Suppl. 1, 4631–4638
14. Shan, T., Xiong, Y., and Kuang, S. (2016) Deletion of Lkb1 in adult mice results in body weight reduction and lethality. *Sci. Rep.* **6,** 36561
15. Zhang, S., Readinger, J. A., DuBois, W., Janka-Junttila, M., Robinson, R., Pruitt, M., Bliskovsky, V., Wu, J. Z., Sakakibara, K., Patel, J., Parent, C. A., Tessarollo, L., Schwartzberg, P. L., and Mock, B. A. (2011) Constitutive reductions in mTOR alter cell size, immune cell development, and antibody production. *Blood* **117,** 1228–1238
16. Lang, G. A., Iwakuma, T., Suh, Y. A., Liu, G., Rao, V. A., Parant, J. M., Valentin-Vega, Y. A., Terzian, T., Caldwell, L. C., Strong, L. C., El-Naggar, A. K., and Lozano, G. (2004) Gain of function of a p53 hot spot mutation in a mouse model of Li-Fraumeni syndrome. *Cell* **119,** 861–872
17. Soukas, A. A., Kane, E. A., Carr, C. E., Melo, J. A., and Ruvkun, G. (2009) Rictor/TORC2 regulates fat metabolism, feeding, growth, and life span in *Caenorhabditis elegans*. *Genes Dev.* **23,** 496–511
18. Liao, Y., Takashima, S., Maeda, N., Ouchi, N., Komamura, K., Shimomura, I., Hori, M., Matsuzawa, Y., Funahashi, T., and Kitakaze, M. (2005) Exacerbation of heart failure in adiponectin-deficient mice due to impaired regulation of AMPK and glucose metabolism. *Cardiovasc. Res.* **67,** 705–713
19. Bergeron, R., Russell, R. R., 3rd, Young, L. H., Ren, J. M., Marcucci, M., Lee, A., and Shulman, G. I. (1999) Effect of AMPK activation on muscle glucose metabolism in conscious rats. *Am. J. Physiol.* **276,** E938–E944
20. Liu, X., Chhipa, R. R., Nakano, I., and Dasgupta, B. (2014) The AMPK inhibitor compound C is a potent AMPK-independent antiglioma agent. *Mol. Cancer Ther.* **13,** 596–605
21. Viollet, B., Horman, S., Leclerc, J., Lantier, L., Foretz, M., Billaud, M., Giri, S., and Andreelli, F. (2010) AMPK inhibition in health and disease. *Crit. Rev. Biochem. Mol. Biol.* **45,** 276–295
22. Li, Y., Xu, S., Mihaylova, M. M., Zheng, B., Hou, X., Jiang, B., Park, O., Luo, Z., Lefai, E., Shyy, J. Y., Gao, B., Wierzbicki, M., Verbeuren, T. J., Shaw, R. J., Cohen, R. A., and Zang, M. (2011) AMPK phosphorylates and inhibits SREBP activity to attenuate hepatic steatosis and atherosclerosis in diet-induced insulin-resistant mice. *Cell Metab.* **13,** 376–388
23. Iizuka, K., and Horikawa, Y. (2008) ChREBP: a glucose-activated transcription factor involved in the development of metabolic syndrome. *Endocr. J.* **55,** 617–624
24. Ota, S., Horigome, K., Ishii, T., Nakai, M., Hayashi, K., Kawamura, T., Kishino, A., Taiji, M., and Kimura, T. (2009) Metformin suppresses glucose-6-phosphatase expression by a complex I inhibition and AMPK activation-independent mechanism. *Biochem. Biophys. Res. Commun.* **388,** 311–316
25. Kohan, A. B., Talukdar, I., Walsh, C. M., and Salati, L. M. (2009) A role for AMPK in the inhibition of glucose-6-phosphate dehydrogenase by polyunsaturated fatty acids. *Biochem. Biophys. Res. Commun.* **388,** 117–121
26. Marini, C., Salani, B., Massollo, M., Amaro, A., Esposito, A. I., Orengo, A. M., Capitanio, S., Emionite, L., Riondato, M., Bottoni, G., Massara, C., Boccardo, S., Fabbi, M., Campi, C., Ravera, S., *et al.* (2013) Direct inhibition of hexokinase activity by metformin at least partially impairs glucose metabolism and tumor growth in experimental breast cancer. *Cell Cycle* **12,** 3490–3499
27. Jäger, S., Handschin, C., St-Pierre, J., and Spiegelman, B. M. (2007) AMP-activated protein kinase (AMPK) action in skeletal muscle via direct phosphorylation of PGC-1α. *Proc. Natl. Acad. Sci. U.S.A.* **104,** 12017–12022
28. Liangpunsakul, S., Ross, R. A., and Crabb, D. W. (2013) Activation of carbohydrate response element-binding protein by ethanol. *J. Investig. Med.* **61,** 270–277
29. Lee, J. M., Seo, W. Y., Song, K. H., Chanda, D., Kim, Y. D., Kim, D. K., Lee, M. W., Ryu, D., Kim, Y. H., Noh, J. R., Lee, C. H., Chiang, J. Y., Koo, S. H., and Choi, H. S. (2010) AMPK-dependent repression of hepatic gluconeogenesis via disruption of CREB·CRTC2 complex by orphan nuclear receptor small heterodimer partner. *J. Biol. Chem.* **285,** 32182–32191
30. Horike, N., Sakoda, H., Kushiyama, A., Ono, H., Fujishiro, M., Kamata, H., Nishiyama, K., Uchijima, Y., Kurihara, Y., Kurihara, H., and Asano, T. (2008) AMP-activated protein kinase activation increases phosphorylation of glycogen synthase kinase 3β and thereby reduces cAMP-responsive element transcriptional activity and phosphoenolpyruvate carboxykinase C gene expression in the liver. *J. Biol. Chem.* **283,** 33902–33910
31. Henriksson, E., Säll, J., Gormand, A., Wasserstrom, S., Morrice, N. A., Fritzen, A. M., Foretz, M., Campbell, D. G., Sakamoto, K., Ekelund, M., Degerman, E., Stenkula, K. G., and Göransson, O. (2015) SIK2 regulates CRTCs, HDAC4 and glucose uptake in adipocytes. *J. Cell Sci.* **128,** 472–486
32. Crescenti, A., del Bas, J. M., Arola-Arnal, A., Oms-Oliu, G., Arola, L., and Caimari, A. (2015) Grape seed procyanidins administered at physiological doses to rats during pregnancy and lactation promote lipid oxidation and up-regulate AMPK in the muscle of male offspring in adulthood. *J. Nutr. Biochem.* **26,** 912–920
33. Lunt, S. Y., and Vander Heiden, M. G. (2011) Aerobic glycolysis: meeting the metabolic requirements of cell proliferation. *Annu. Rev. Cell Dev. Biol.* **27,** 441–464
34. Piletz, J. E., Ivanov, T. R., Sharp, J. D., Ernsberger, P., Chang, C. H., Pickard, R. T., Gold, G., Roth, B., Zhu, H., Jones, J. C., Baldwin, J., and Reis, D. J. (2000) Imidazoline receptor antisera-selected (IRAS) cDNA: cloning and characterization. *DNA Cell Biol.* **19,** 319–329
35. Zhang, L., Zhao, T. Y., Hou, N., Teng, Y., Cheng, X., Wang, B., Chen, Y., Jiang, L., Wu, N., Su, R. B., Yang, X., and Li, J. (2013) Generation and primary phenotypes of imidazoline receptor antisera-selected (IRAS) knockout mice. *CNS Neurosci. Ther.* **19,** 978–981
36. Hedman, A. C., Smith, J. M., and Sacks, D. B. (2015) The biology of IQGAP proteins: beyond the cytoskeleton. *EMBO Rep.* **16,** 427–446
37. Watanabe, T., Wang, S., and Kaibuchi, K. (2015) IQGAPs as key regulators of actin-cytoskeleton dynamics. *Cell Struct. Funct.* **40,** 69–77
38. Benseñor, L. B., Kan, H. M., Wang, N., Wallrabe, H., Davidson, L. A., Cai, Y., Schafer, D. A., and Bloom, G. S. (2007) IQGAP1 regulates cell motility by linking growth factor signaling to actin assembly. *J. Cell Sci.* **120,** 658–669
39. White, C. D., Erdemir, H. H., and Sacks, D. B. (2012) IQGAP1 and its binding proteins control diverse biological functions. *Cell. Signal.* **24,** 826–834
40. Sayedyahossein, S., Li, Z., Hedman, A. C., Morgan, C. J., and Sacks, D. B. (2016) IQGAP1 binds to yes-associated protein (YAP) and modulates its transcriptional activity. *J. Biol. Chem.* **291,** 19261–19273
41. Chawla, B., Hedman, A. C., Sayedyahossein, S., Erdemir, H. H., Li, Z., and Sacks, D. B. (2017) Absence of IQGAP1 protein leads to insulin resistance. *J. Biol. Chem.* **292,** 3273–3289
42. Lehtonen, S., Ryan, J. J., Kudlicka, K., Iino, N., Zhou, H., and Farquhar, M. G. (2005) Cell junction-associated proteins IQGAP1, MAGI-2, CASK, spectrins, and α-actinin are components of the nephrin multiprotein complex. *Proc. Natl. Acad. Sci. U.S.A.* **102,** 9814–9819
43. Rittmeyer, E. N., Daniel, S., Hsu, S. C., and Osman, M. A. (2008) A dual role for IQGAP1 in regulating exocytosis. *J. Cell Sci.* **121,** 391–403
44. Kimura, T., Yamaoka, M., Taniguchi, S., Okamoto, M., Takei, M., Ando, T., Iwamatsu, A., Watanabe, T., Kaibuchi, K., Ishizaki, T., and Niki, I. (2013) Activated Cdc42-bound IQGAP1 determines the cellular endocytic site. *Mol. Cell. Biol.* **33,** 4834–4843
45. Smith, A. C., Bruce, C. R., and Dyck, D. J. (2005) AMP kinase activation with AICAR simultaneously increases fatty acid and glucose oxidation in resting rat soleus muscle. *J. Physiol.* **565,** 537–546
46. Meng, X., Guo, J., Fang, W., Dou, L., Li, M., Huang, X., Zhou, S., Man, Y., Tang, W., Yu, L., and Li, J. (2016) Liver microRNA-291b-3p promotes hepatic lipogenesis through negative regulation of adenosine 5′-monophosphate (AMP)-activated protein kinase α1. *J. Biol. Chem.* **291,** 10625–10634
47. Horton, J. D., Goldstein, J. L., and Brown, M. S. (2002) SREBPs: activators of the complete program of cholesterol and fatty acid synthesis in the liver. *J. Clin. Invest.* **109,** 1125–1131
48. Wang, Y., Inoue, H., Ravnskjaer, K., Viste, K., Miller, N., Liu, Y., Hedrick, S., Vera, L., and Montminy, M. (2010) Targeted disruption of the CREB

coactivator Crtc2 increases insulin sensitivity. *Proc. Natl. Acad. Sci. U.S.A.* **107,** 3087–3092

49. Tran, L., Zielinski, A., Roach, A. H., Jende, J. A., Householder, A. M., Cole, E. E., Atway, S. A., Amornyard, M., Accursi, M. L., Shieh, S. W., and Thompson, E. E. (2015) Pharmacologic treatment of type 2 diabetes: oral medications. *Ann. Pharmacother.* **49,** 540–556
50. Zhou, G., Myers, R., Li, Y., Chen, Y., Shen, X., Fenyk-Melody, J., Wu, M., Ventre, J., Doebber, T., Fujii, N., Musi, N., Hirshman, M. F., Goodyear, L. J., and Moller, D. E. (2001) Role of AMP-activated protein kinase in mechanism of metformin action. *J. Clin. Invest.* **108,** 1167–1174
51. Benhamed, F., Denechaud, P. D., Lemoine, M., Robichon, C., Moldes, M., Bertrand-Michel, J., Ratziu, V., Serfaty, L., Housset, C., Capeau, J., Girard, J., Guillou, H., and Postic, C. (2012) The lipogenic transcription factor ChREBP dissociates hepatic steatosis from insulin resistance in mice and humans. *J. Clin. Invest.* **122,** 2176–2194
52. Petrescu, I., Bojan, O., Saied, M., Bârzu, O., Schmidt, F., and Kühnle, H. F. (1979) Determination of phosphoenolpyruvate carboxykinase activity with deoxyguanosine 5′-diphosphate as nucleotide substrate. *Anal. Biochem.* **96,** 279–281
53. Wiese, T. J., Lambeth, D. O., and Ray, P. D. (1991) The intracellular distribution and activities of phosphoenolpyruvate carboxykinase isozymes in various tissues of several mammals and birds. *Comp. Biochem. Physiol. B* **100,** 297–302
54. Frayn, K. N. (1983) Calculation of substrate oxidation rates *in vivo* from gaseous exchange. *J. Appl. Physiol. Respir. Environ. Exerc. Physiol.* **55,** 628–634